IOPscience iopscience.iop.org

Home Search Collections Journals About Contact us My IOPscience

The infrared activity of polyacetylene

This article has been downloaded from IOPscience. Please scroll down to see the full text article.

1994 J. Phys.: Condens. Matter 6 5577

(http://iopscience.iop.org/0953-8984/6/28/028)

View the table of contents for this issue, or go to the journal homepage for more

Download details:
IP Address: 171.66.16.147
The article was downloaded on 12/05/2010 at 18:55

Please note that terms and conditions apply.

J. Phys.: Condens. Matter 6 (1994) 5577–5600. Printed in the UK

The infrared activity of polyacetylene

C Benoit, G Poussigue, J Elmachtani-Idrissi and R Bichri El Alaoui

Groupe de Dynamique des Phases Condensées URA 233-cp026, Université Montpellier II, Place E Bataillon, 34095 Montpellier Cédex 05, France

Received 14 March 1994

Abstract. In this paper, we study the dynamic and infrared activity of pure *trans*- and *cis*-polyacetylene, doped systems, and systems with *cis–trans* defects. First we study the behaviour of the Goldstone mode frequency of a simple linear chain. We find that this frequency depends strongly on the value of the dimerization parameter u, in contrast with the experimental results, where this mode is particularly stable. Thus, taking u as a free parameter, we develop several realistic models for neutral perfect *cis* and *trans* chains and doped systems. Our results are in very good agreement with experimental results. We show that for the doped chain the transverse component of conductivity is about 1% of the longitudinal component. The presence of the *cis–trans* defect allows us to give the origin of several peaks found experimentally and not interpreted until now. We show that in the presence of *cis–trans* defects the photoinduced infrared activity may appear in systems with charged solitons and antisolitons on the same neutral chain. Computed results are also in very good agreement with the experimental data.

1. Introduction

Among the conducting polymers, polyacetylene $(CH)_x$ has been the most intensively investigated. Polyacetylene is a linear conjugated polymer and, because of the degenerate ground state of its structure, excitations in the form of topological defects are expected. Local excitations, solitons and polarons, in $t-(CH)_x$ have attracted much interest, and although up to now a great number of papers on polyacetylene have appeared, the exact role played by topological excitations, disorder, and defects is still under discussion. However it is now well known that, under doping, strong infrared (IR) bands appear; these bands are nearly independent of the dopant species, and they undergo the isotopic effect. Also, it is believed that this absorption arises from the formation of localized structural distortions with associated localized vibrational modes. In consequence, these effects have been to date, with the photoinduced IR activity, one of the best signatures of the existence of charged defects. The IR properties of doped materials and the photoinduced IR activity have been discussed at length in a review paper (Benoit *et al* 1990). The authors have shown that, although an important dispersion was observed within the experimental results, after several years some standardization has occurred and a number of experimental facts are actually well established concerning the doped material: two main absorption bands appear in $(CH)_x$ in the regions 500–1000 cm^{-1} and 1360–1400 cm^{-1} with a higher occurrence in 850–900 cm^{-1} and 1370–1390 cm^{-1} regions. These bands as well as their relative intensities are almost independent of the nature and even type (p or n) of the dopant. For a given dopant species, the position of the 900 cm^{-1} mode is following the studied samples: either almost independent of the dopant concentration (most usual) or strongly dependent (until $\Delta\omega/\omega \simeq 30\%$ (Kim and Heeger 1989)). No effect related to the *trans*

0953-8984/94/285577+24$19.50 © 1994 IOP Publishing Ltd

chain length is observed by IR spectroscopy; for example these bands have been observed with a comparable intensity in segmented $(CH)_x$. Finally, these bands subsist even at very high doping level (in the metallic range). The two main absorption bands are also observed by the photoinduced effect at low temperature. In $(CH)_x$ the low-frequency one is shifted down to 500 cm^{-1}.

On the other hand, many models have been developed to interpret these modes; most of them are derived from the SSH model (Su, Schrieffer and Heeger 1979, 1980). In the SSH model of polyacetylene, which incorporates electron–phonon coupling into a tight-binding Hamiltonian, charges added to the chain, either through charge transfer doping or following photoexcitation, break the dimerization pattern, leading to the creation of spinless charged domain walls or solitons separating sections of chain with opposite bond alternation. Mele and Rice (1980) and Mele (1981) developed the first discrete model to describe a $(CH)_x$ chain containing a soliton and to interpret the IR absorption spectra. Zannoni and Zerbi (1982a, b) studied the dynamics of a $(CH)_x$ chain containing a regular or a random distribution of centrosymmetrical defects. Takayama, Lin-Liu and Maki (TLM) (1980) developed a model that is a continuum version of the SSH model and allows us to analyse the soliton behaviour in a one-dimensional charge density wave system with a half-filled electron band. Horovitz (1982) studied the optical behaviour, especially concerning IR and Raman spectroscopy, of lightly doped $(CH)_x$. This model is a multibranch version of the TLM model. After these, many models have been developed, discrete or continuous, with one-phonon or multiphonon branches. Hicks and Blaisdell (1985), Ito *et al* (1984), Terai *et al* (1985a, b), and Terai and Ono (1986) calculated the phonon modes for a $(CH)_x$ chain containing a soliton or a polaron. Ito *et al* (1984) and Ito and Ono (1985) have analysed the small lattice oscillations around a soliton and used these results to study the optical conductivity. Sun *et al* (1985) started from the SSH model and found five localized linear modes for a soliton, while Chao and Wang (1985) found eight localized modes, Mele and Hicks (1985), Hicks and Mele (1986), Terai *et al* (1986), and Hicks and Tinka Gammel (1986) developed, in order to build a more realistic model, three-component Hamiltonians. Hicks *et al* (1987) performed calculations similar to those of Terai and Ono (1986) in order to interpret the photoexcitation data and obtained very similar results. Hicks and Tinka Gammel (1988) and Shuai *et al* (1993) studied the effect of Hubbard interaction and electrostatic pinning of two solitons on neighbouring chains. Recently vibrational modes around a moving solition have been studied by Kuwabara and Ono (1993) and Zhen Ye (1992). However, and whatever the difficulties concerning the two (or three) infrared active vibrational (IRAV) modes, one of them seems to be correctly interpreted by all models, in terms of the frequencies as well as the relative intensities: the 1390 cm^{-1} one, whose origin is very well defined. The mode at 1290 cm^{-1}, interpreted as an IRAV mode in many papers, is assigned to a defect mode by several authors. One of the most important questions concerns the assignment of the third strong absorption band: the 900 cm^{-1} mode. All the continuous models, and even the discrete ones, except those of Mele and Rice (1980), Mele (1981), and Zannoni and Zerbi (1982a, b) assign the 900 cm^{-1} absorption band to the Goldstone mode whose frequency is shifted by a potential produced by the impurities (counterions) or by the coulombic attraction in the photoinduced effect. However this hypothesis leads to some contradictions, as follows.

(i) The Goldstone mode implies energy invariance when the defect is moved; a mode of this kind appears improbable in a segmented chain of 10 carbon atoms.

(ii) The frequency of this mode is nearly invariant when the doping level is increased. However, we have seen that, from the softening of the pinning potential, the frequency of such a mode should be shifted towards zero (Benoit *et al* 1983). Such an effect is not observed. Mostly it decreases lightly and occasionally it increases.

(iii) The frequency of this mode is nearly invariant with the doping species, whatever its size and structure, the doping methods, and the preparation of the samples.

(iv) The IRAV modes persist in the metallic state where they should disappear.

Thus the origin of the enhanced IRAV modes intensities in heavily doped polyacetylene remains an important unresolved problem (Heeger *et al* 1988, Kim and Heeger 1989).

Following the conclusion of Benoit *et al* (1983) we deduce that the 900 cm^{-1} mode arises from a strong localization of motion of the Goldstone mode, which should be determined.

In this paper we develop realistic models in order to interpret the origin of these different bands. In section 2 we study the *trans* structure. We study first a pure linear chain and the behaviour of the Goldstone mode frequency when parameters are changed. We find that this frequency is strongly dependent on the dimerization parameter and thus very sensitive to the minimization of energy. Taking these results into account we develop models for the perfect *trans* planar chain and for doped systems, the dimerization parameter being evaluated as the other parameters by using a fitting method. We develop, in section 3, models for the planar *cis* isomer. In section 4 we study the dynamic and the IR conductivity of the *cis–trans* defect.

2. *Trans*-polyacetylene

To model the polyacetylene we assume the SSH Hamiltonian for the electronic properties and a classical force field model for the short-range forces. The potential is extended in terms of internal coordinates, which take into account the exact structure of the chain. In the SSH Hamiltonian, the following approximations are made: the interchain coupling is neglected so that $(CH)_x$ is considered as a quasi-one-dimensional system; σ electrons are treated with an adiabatic approximation; π electrons are treated in a tight-binding approximation with a hopping integral $t_{n+1,n}$. Then the Hamiltonian is given by

$$\mathbf{H}_{\text{trans}} = \mathbf{H}_{\text{trans}}^{\text{elect}} + \mathbf{H}_{\text{trans}}^{\text{elast}} + \tfrac{1}{2}\sum_{n,\alpha} m_n \dot{u}_{\alpha n}^2 \tag{1}$$

where the electronic Hamiltonian part is given by

$$\mathbf{H}_{\text{trans}}^{\text{elect}} = -\sum_{n,s} t_{n+1,n}(c_{n+1,s}^{+} c_{n,s} + c_{n,s}^{+} c_{n+1,s}). \tag{2}$$

The operator $c_{n,s}^{+}(c_{n,s})$ creates (annihilates) a π electron of spin $s(\pm\frac{1}{2})$ on the nth carbon; m_n is the mass of the nth atom. The elastic Hamiltonian is given by

$$\mathbf{H}_{\text{trans}}^{\text{elast}} = \tfrac{1}{2}\sum_{ij} K_{ij}\xi_i\xi_j \tag{3}$$

where K_{ij} represent the short-range force constants for the σ bond and ξ_i the internal coordinates. In the presence of electron–phonon coupling, the hopping energy is expanded as

$$t_{n,n+1} = t_{n,n+1}^{0} - \alpha\Delta\rho_n \tag{4}$$

where $t_{n,n+1}^{0}$ is the hopping integral for the undisturbed chain, α the electron–phonon coupling constant, and $\Delta\rho_n$ the change of the length of the carbon–carbon bond. In order to obtain the dynamics matrix we compute the phonon Green functions of the system in the presence of electron–phonon coupling.

2.1. Dynamical theory

We consider first the short-range forces or elastic part of the Hamiltonian. If ξ_n represents one of the internal coordinates and $u_\alpha(n)$ one of the Cartesian displacement coordinates, the relations are in the form

$$\xi_n = \sum_{\alpha,m} d(n, \alpha m) u_\alpha(m) \tag{5}$$

where the coefficients $d(n, \alpha m)$ are constants determined by the structure of the system. The elastic part of the dynamical matrix is then given in Cartesian coordinates by

$$\Phi = \mathbf{M}^+\mathbf{d}^+\mathbf{K}\mathbf{d}\mathbf{M} \tag{6}$$

where $\mathbf{M}$ is the inverse squared root mass matrix. For large system, the computation of (6) is very time consuming. The use of the technique developed with a sparse matrix (Benoit *et al* 1992) allows us to evaluate (6) with a very reasonable computing time. Thus these coefficients are evaluated exactly for every structure studied in this work: pure *cis* and *trans* chains, chains with solitons, and *cis–trans* defects. For the evaluation of long-range forces, we write the electronic Hamiltonian as

$$\mathbf{H}_{\text{trans}} = \mathbf{H}^0_{\text{trans}} + \mathbf{H}_1 \tag{7}$$

where $\mathbf{H}^0_{\text{trans}}$ is the Hamiltonian of the undisturbed system and

$$\mathbf{H}_1 = \sum_{n,s} \alpha[c^+_{n+1,s}c_{n,s} + c^+_{n,s}c_{n+1,s}]\Delta\rho_n \tag{8}$$

and from (5)

$$\Delta\rho_n = \sum_{\alpha,m} d(n, \alpha m) u_\alpha(m) \tag{9}$$

with $\Delta\rho_n \equiv \xi_n$ for $n = 1, N$; N is the number of carbon atoms. In the described model the phonon Green functions are given by

$$G(u_n(\tau), u_{n'}(0)) = -\frac{\langle \mathbf{T} u_n(\tau) u_{n'}(0) \mathbf{S}(\beta\hbar, 0)\rangle}{\langle \mathbf{S}(\beta\hbar, 0)\rangle} \tag{10}$$

where τ is the imaginary time, $\beta = 1/kT$, $\mathbf{T}$ is the ordering time operator and

$$\mathbf{S}(\beta\hbar, 0) = 1 - \frac{1}{\hbar}\int_0^{\beta\hbar} H_1^i(\tau_1)\,\mathrm{d}\tau_1 + \frac{1}{2\hbar^2}\int_0^{\beta\hbar}\int_0^{\beta\hbar} \mathbf{T}(H_1^i(\tau_1)H_1^i(\tau_2))\,\mathrm{d}\tau_1\,\mathrm{d}\tau_2 + \ldots \tag{11}$$

where $H_1^i(\tau)$ is in interaction representation. From the Dyson equation, one obtains for the Green propagator

$$\mathbf{G}^{-1} = (\mathbf{G}^0)^{-1} - \mathbf{\Pi} \tag{12}$$

where $\mathbf{\Pi}$ is the polarization (Abrikosov *et al* 1963) and

$$(\mathbf{G}^0)^{-1} = \mathbf{D}^0 - \omega^2\mathbf{I} \tag{13}$$

is the undisturbed Green function. The polarization Π is given by

$$\Pi_{\alpha\beta}(m_1, m_2, \omega, T) = 2\beta\alpha^2 \sum_{j_1, j_2, n_1, n_2} d(n_1, \alpha m_1) B(j_1, j_2, n_1) B(j_2, j_1, n_2) \times \frac{n_{j_1} - n_{j_2}}{i\hbar\omega - (E_{j_2} - E_{j_1})} d(n_2, \beta m_2) \tag{14}$$

where summation on the spin states has been taken into account and

$$B(j_1, j_2, n) = \langle n|j_1\rangle\langle j_2|n+1\rangle + \langle n+1|j_1\rangle\langle j_2|n\rangle \tag{15}$$

$\langle m|j\rangle$ is the mth component of the $|j\rangle$ state and $n_j = 1/(e^{-\beta E_j} - 1)$ is the Fermi occupation number.

In the adiabatic approximation ($\omega \ll E_g$) and at $T = 0$ K, the elements of the matrix Π are given, in Cartesian coordinates, by

$$\Pi_{\alpha\beta}(m_1, m_2) = -4\alpha^2\beta \sum_{n_1, n_2} \sum_{j_1, j_2} d(n_1, \alpha m_1) B(j_1, j_2, n_1) B(j_2, j_1, n_2) \frac{1}{(E_{j_1} - E_{j_2})} d(n_2, \beta m_2) \tag{16}$$

where the summations over j_1 concern all filled states and those over j_2 all empty states.

The dynamic matrix of the system is given by

$$\mathbf{D} = \mathbf{D}^0 - \mathbf{\Pi} \tag{17}$$

where $\mathbf{D}^0$ is the dynamic matrix without electron–phonon coupling. The squares of the frequencies are the poles of the Green function or the zeros of $\mathbf{G}^{-1}$ and so the eigenvalues of $\mathbf{D}$.

2.2. *Optical conductivity*

We study now the IR absorption of charged chains. The IR conductivity is generally computed along the chain. However, it was interesting to take into account the exact structure of the chain and to compute the activity parallel to but also perpendicular to the chain. The conductivity tensor is given by

$$\sigma_{\alpha\beta}(\omega) = (1/i\omega)\chi_{\alpha\beta}(\omega) \tag{18}$$

where $\chi_{\alpha\beta}(\omega)$ is the Fourier transform of $\chi_{\alpha\beta}(t - t')$, which is the susceptibility tensor coupling the current density to the potential vector of the electromagnetic field. Using the imaginary time technique it is known that

$$\chi_{\alpha\beta}(\tau) = \chi(j_\alpha, j_\beta, \tau) = \beta\mathbf{G}(j_\beta, j_\alpha\tau) \tag{19}$$

where $-\beta\hbar < \tau < \beta\hbar$ and $\mathbf{G}(j_\beta, j_\alpha, \tau)$ is the current–current correlation function. With the Hamiltonian (7) the current operator is given by

$$j_\alpha = -\frac{ie}{m\hbar} \sum_{n,s} (r_{n+1,\alpha} - r_{n,\alpha}) t_{n,n+1} [c^+_{n+1,s} c_{n,s} + c^+_{n,s} c_{n+1,s}] \tag{20}$$

where r_n is the position of the nth atom. Using the Matsubara (1956) technique, one obtains, in the adiabatic approximation ($\omega \ll E_g$), at $T = 0$ K, for the conductivity

$$\sigma_{\alpha\beta}(\omega) = \frac{e^2\alpha^2\pi}{4m^2\hbar^2}\sum_q \mathcal{T}_\alpha(q)\mathcal{T}_\beta(q)[\delta(\omega-\omega_q)-\delta(\omega+\omega_q)] \tag{21}$$

where

$$\mathcal{T}_\alpha(q) = \sum_{\gamma m}\frac{Q_{\alpha\gamma}(m)}{\sqrt{m_m}}e_{\gamma m}(q) \tag{22}$$

with $Q_{\alpha\gamma}(m)$ given by

$$Q_{\alpha\gamma}(m) = \sum_{\substack{j_1\text{filled}\\ j_2\text{empty}}}\frac{A_\alpha(j_1,j_2)}{(E_{j_1}-E_{j_2})^2}\sum_n B(j_1,j_2,n)d(n,\gamma m) \tag{23}$$

and

$$A_\beta(j_1,j_2) = \sum_n t_{n,n+1}\Delta r_{n\beta}[\langle j_1|n+1\rangle\langle n|j_2\rangle - \langle j_1|n\rangle\langle n+1|j_2\rangle] \tag{24}$$

with

$$\Delta r_{n\beta} = (r_{n+1,\beta} - r_{n,\beta}). \tag{25}$$

We note that the expression (21) for the conductivity is very close to the classical form (see later equations (41), (42)) for the IR susceptibility, but charges $Q_{\alpha\gamma}(m)$ now appear from the electron–phonon coupling. Expression (21) is in agreement with the equation found by Hicks and Tinka Gammel (1986, 1988) in a pure 1D system ($\alpha = \gamma = z$).

2.3. *Application to pure 1D model*

Each C–H group is described by one dimerization coordinate u_n. The Hamiltonian is always given by (1) but now with the elastic energy given by

$$\mathsf{H}_{\text{trans}}^{\text{elast}} = \frac{1}{2}\mathsf{K}\sum_n (u(n+1)-u(n))^2 \tag{26}$$

where from (9) $d(n,m) = 1$ if $m = n+1$, -1 if $m = n$, 0 otherwise.

The polarization Π and the conductivity are obtained from (16) and (21)–(23) but only the Cartesian component parallel to the chain is taken into account. The $\mathbf{D}^0$ part of the dynamical matrix, without electron–phonon coupling (with $\beta = 1$), is given by

$$\mathbf{D}^0_{m,n} = \mathsf{K}(2\delta_{m,n} - \delta_{m,n-1} - \delta_{m,n+1}). \tag{27}$$

Computation of the optical conductivity has been performed with 201-site chains with $t_0 = 2.5$ eV, $K = 21$ eV Å^{-2}. According to the SSH model, we have introduced the order parameter

$$\Psi_n = (-1)^n u_n. \tag{28}$$

The total energy has been minimized using the functions

$$\Psi_n = -u_0 \tanh(n/l) + \delta(\phi(n)). \tag{29}$$

To study the localization of the eigenmodes we have calculated the localization entropy, which is directly related to the lack of information concerning the position of the phonons in the system. The localization entropy is given by

$$S(\omega) = \sum_q S_q \delta(\omega - \omega_q) \tag{30}$$

where

$$S_q = -\frac{1}{\log(N)} \sum_n P_n(q) \log(P_n(q)) \tag{31}$$

with

$$P_n(q) = |\langle n|q\rangle|^2. \tag{32}$$

Log(N) is a normalization factor such that $S(\omega) = 1$ for the extended modes. The value of this function for a chain of 201 atoms in the presence of a soliton is reported in figure 1. There are always five strongly localized modes $\omega_0 = 0.4$ cm^{-1} (Goldstone mode), $\omega_1 = 707$ cm^{-1}, $\omega_2 = 832$ cm^{-1}, $\omega_3 = 924$ cm^{-1}, $\omega_4 = 1083$ cm^{-1}. The shape of the modes is nearly identical to those obtained previously by other authors (Terai and Ono 1986, Hicks and Tinka Gammel 1986). The ω_4 mode is due to the finite size of the chain. This result has been already mentioned by Terai and Ono (1986). The conductivity is reported in figure 2. We note that two modes are IR active. We note also an IR activity in the low-frequency regime near the Goldstone mode. This result, which has been pointed out by several authors (Nakahara and Maki 1982, Terai and Ono 1986) is explained by Hicks and Tinka Gammel (1986) as arising from a transfer of the conductivity of the Goldstone mode to the acoustic phonons.

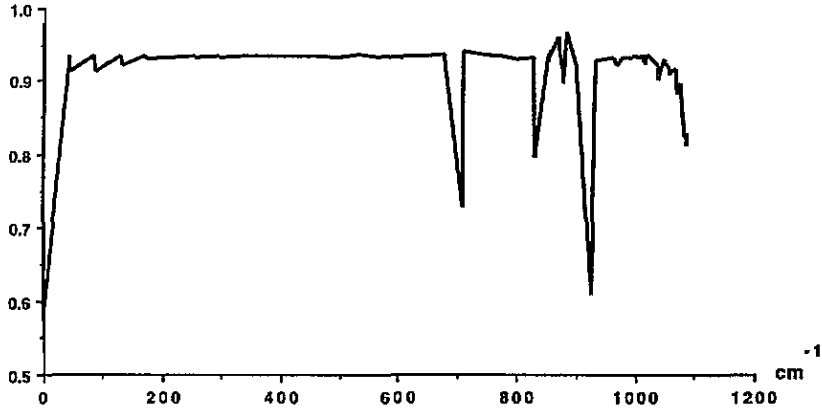

Figure 1. The localization entropy of a 201-site chain. For a perfectly extended mode $S(\omega) = 1$. $S(\omega)$ is weaker the more the mode is localized.

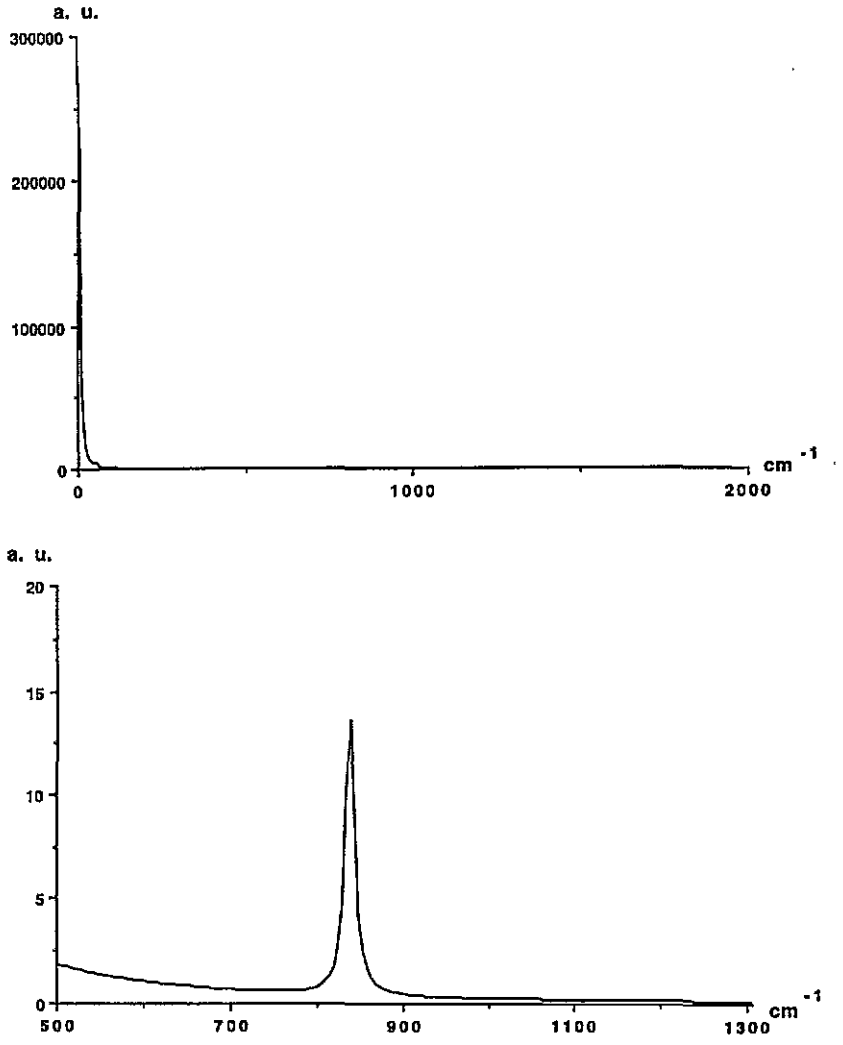

Figure 2. The IR conductivity in 1D $(CH)_x$ for a 201-site chain: top, the whole spectrum; bottom, a detail in the 500–1200 cm^{-1} region.

The frequency of the Goldstone mode versus the dimerization parameter u for the 101- and 201-site chains is reported in figure 3. We note that a very small change in the value of the parameter u strongly changes the frequency of the Goldstone mode. Thus the frequency of this mode will be very sensitive to any small perturbation of the translational invariance of the chain.

In real systems, we have seen that the 900 cm^{-1} mode is very stable with doping, presence of defects, and change in temperature. A simple conclusion is that the high-frequency value of this mode arises from an intrinsic pinning of the soliton, even in the absence of the coulombic potential. This pinning could arise from any defect that breaks the infinitesimal translation invariance of the chain and perturbs the value of the dimerization parameter u: tridimensional effects conjugated with the zig-zag discrete structure of the real chains, confinement of the solitons due to 3D interactions (Baughman and Moss 1982, Maki

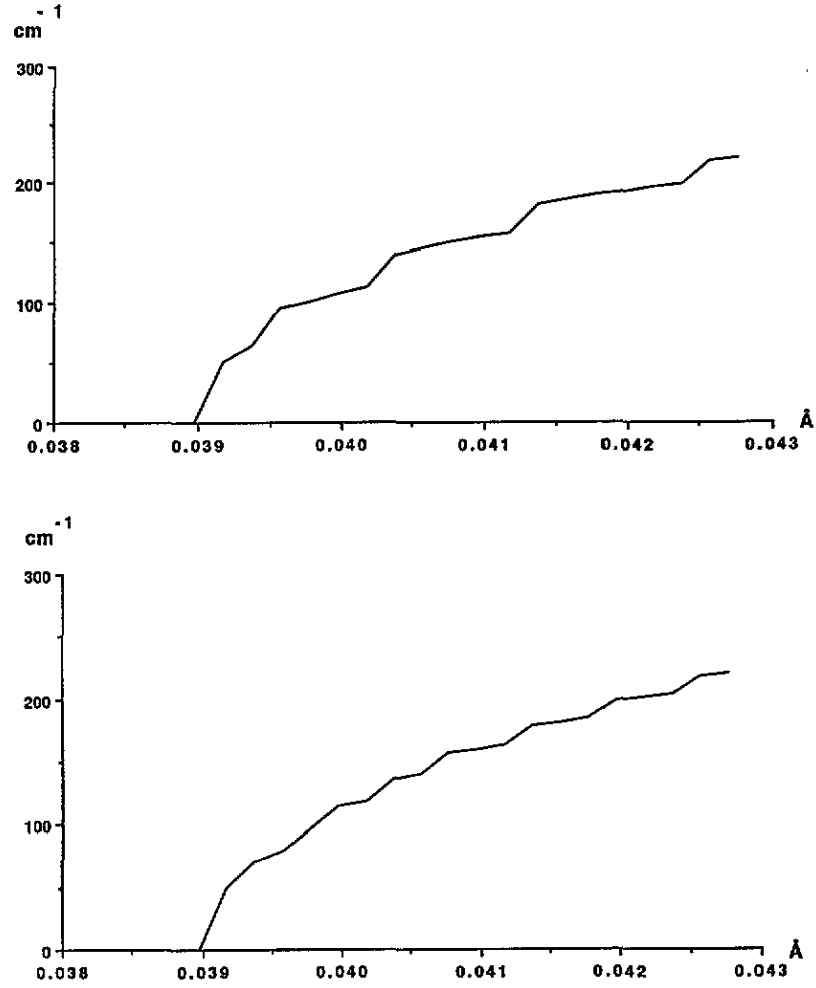

Figure 3. The variation of the Goldstone mode frequency with the dimerization parameter for a 101-site chain (top) and a 201-site chain (bottom).

1984), interaction with structural defects, torsion of the chain, and so forth.

Keeping in mind that minimization of the free energy of real systems in order to evaluate the values of parameters of models is beyond the possibilities of actual computational techniques, a simple method to represent pinning of the soliton is to take u as a free parameter, fixed by comparison with experimental data. We shall use this possibility in the following sections.

2.4. Planar trans structure

2.4.1. Perfect chain. We consider the Hamiltonian (1), the internal coordinates ξ_i being given in figure 4. We assume that the transfer integral and elastic constants can be expanded in terms of the dimerization pattern in the following way:

$$t_{n,n+1} = t^0 - \alpha\Delta\bar{\rho}_n \tag{33}$$

Table 1. Elastic constants of *trans*-polyacetylene.

Force constants (mdyn Å^{-1}, mdyn, mdyn Å)			
$K(a_1^2)$	6.77	$K(\alpha_2^2)$	1.1
$K(a_2^2)$	7.96	$K(\alpha_1\alpha_2)$	−0.1
$K(a_1a_1)$	0.2	$K(\alpha_2\alpha_1)$	0.1
$K(a_2a_2)$	0.49	$K(a_1\alpha_2)$	0.14
$K(a_1a_2)$	0.497	$K(a_2\alpha_2)$	0.36
$K(b_1^2)$	4.92	$K(\varphi_1^2)$	1.1
$K(a_1b_2)$	0.15	$K(a_1\varphi_1)$	0.2
$K(a_2b_2)$	0.55	$K(a_2\varphi_1)$	−0.35

and

$$K_{ij} = K_{ij}^0 - \sum_n (K_{ij,n}\Delta\bar{\rho}_n) \tag{34}$$

where t^0 and K_{ij}^0 are the transfer integral and elastic constants of the undimerized chain, and $\Delta\bar{\rho}_n = (-1)^{n+1}(\bar{\Psi}_{n+1} + \bar{\Psi}_n)$, the static distortion of the chain.

For a dimerized system (a perfect *trans* chain) the order parameter is such that $\bar{\Psi}(n) = \pm u_0$. For the fitting procedure we have used the IR results of Shirakawa and Ikeda (1971) and Galtier *et al* (1984), while for the Raman data we have used the results of Schügerl and Kuzmany (1981) and Faulques (1990). The parameters of the electronic Hamiltonian are $\alpha = 5.7$ eV Å^{-1}, $t_0 = 2.5$ eV, $u_0 = 0.032$ Å, which give a gap of 1.46 eV. The parameters of the *trans* structure are taken as $l_{C-C} = 1.46$ Å, $l_{C=C} = 1.34$ Å, $l_{C-H} = 1.09$ Å, $\theta(C=C-H) = \alpha(C=C-C) = 120°$. Values of elastic constants of the dimerized chain are reported in table 1. Tables 2 and 3 compare experimental to calculated modes for $(CH)_x$ and $(CD)_x$, respectively, for the present work and Faulques' work (1990). It is clear that agreement with the present work is rather good. Dispersion curves are reported in figures 5 and 6. We note the strong dispersion of the Raman active modes ν_5 and ν_6 in agreement with results of Mele and Rice (1980) and Mulazzi *et al* (1983).

Table 2. Theoretical and experimental frequencies of *trans*-$(CH)_x$.

	Experimental frequencies		Theoretical frequencies	
	Shiratawa and Ikeda (1971)	Galtier *et al* (1984)	Faulques (1990)	Present work
	—	1253	—	—
Bu	1292	1292 (def)	1281	1293
	3013	3011	3020	3004
	Schügerl and Kuzmany (1981)	Faulques (1990)	Faulques (1990)	Present work
	1060	1064	1055	1080
Ag	1285	1294	1281	1317
	1450	1456	1447	1410
	2990	—	2993	3000

2.4.2. Doped systems. We consider a chain with a soliton and an antisoliton. The static order parameter, which represents the change in bond length is given by

$$\Psi(n) = u_0 \tanh[(n - n_1)/l]\tanh[(n - n_2)/l] \tag{35}$$

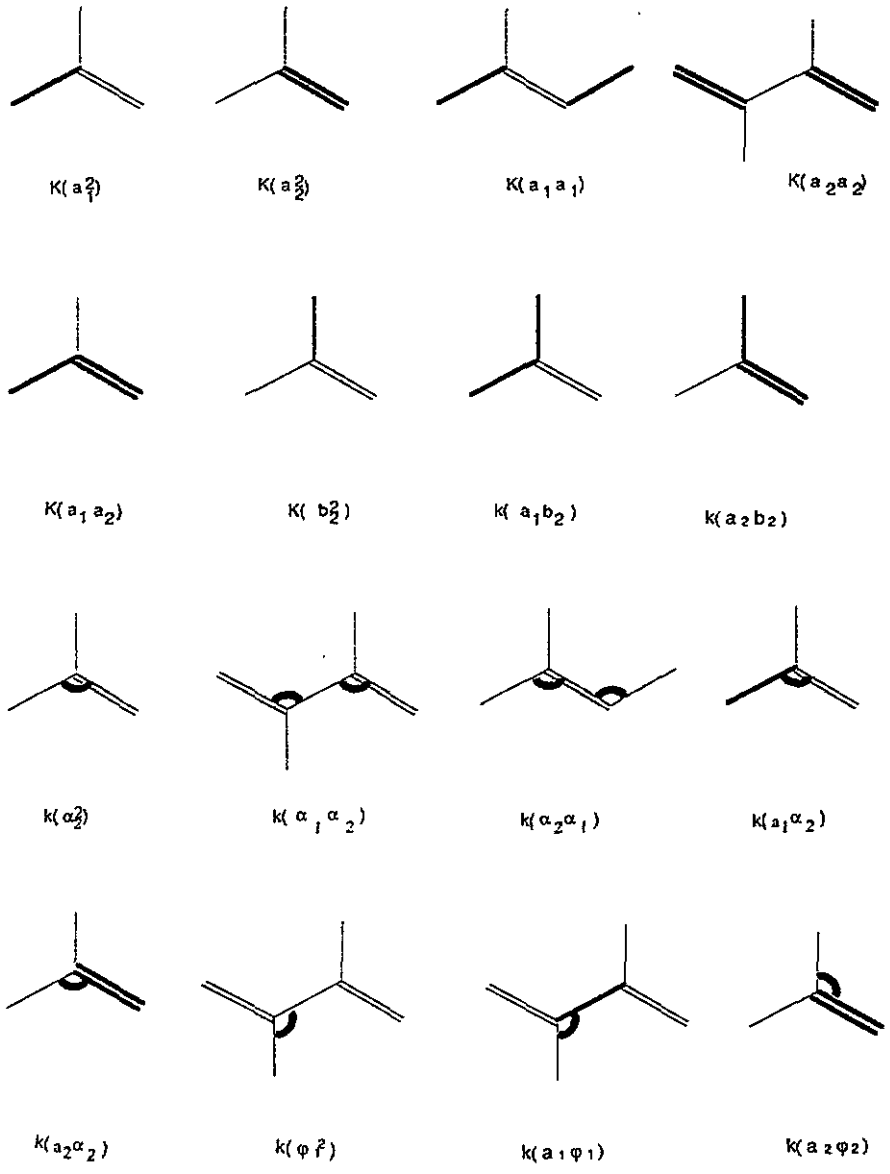

Figure 4. Internal coordinates for *trans*-polyacetylene force constants.

where n_1 and n_2 give the positions of the soliton and antisoliton. The coulombic pinning is modelled as a point charge off the chain. The Hamiltonian of the chain is now given by (Hicks and Tinka Gammel 1988)

$$\mathbf{H}_{\text{trans}} = \mathbf{H}_{\text{trans}} + \sum_{n,s} V(n)(c^{+}_{n,s}c_{n,s} - \tfrac{1}{2}) \tag{36}$$

where $V(n)$ is the coulombic potential given by

$$V(n) = -\frac{e^2}{\varepsilon_1\sqrt{\varepsilon_2}} \sum_{n_s=1}^{2} \frac{1}{R_{n,n_s}} \exp(-\Lambda R_{n,n_s}). \tag{37}$$

Table 3. Theoretical and experimental frequencies of *trans*-$(CD)_x$.

	Experimental frequencies		Theoretical frequencies	
	Shirakawa and Ikeda (1971)	Galtier *et al* (1984)	Faulques (1990)	Present work
Bu	916	910	940	949
	2231	2235	2218	2205
	Schügerl and Kuzmany (1981)	Faulques (1990)	Faulques (1990)	Present work
	840	852	808	842
Ag	1200	1204	1221	1201
	1340	1344	1338	1334
	2230	—	2216	2236

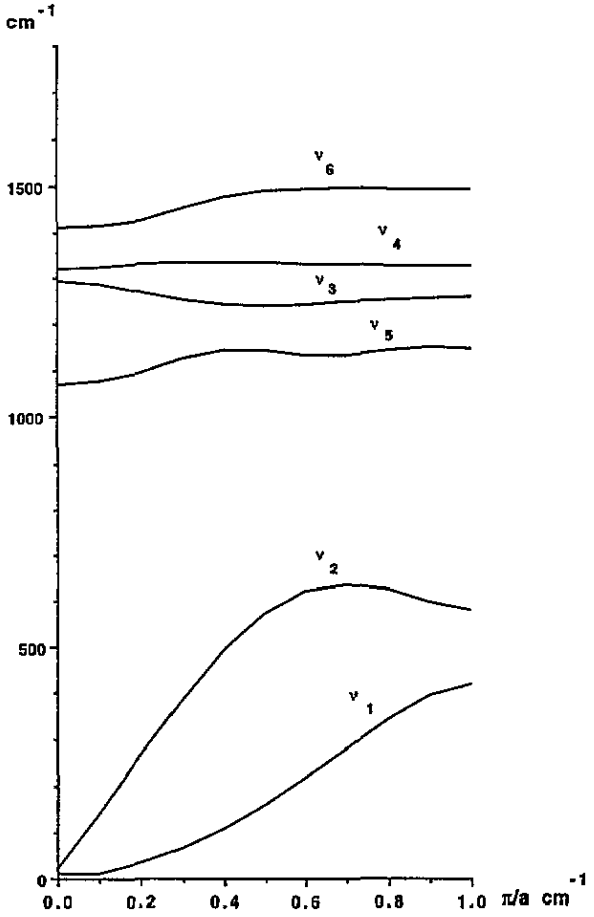

Figure 5. Dispersion curves for *trans*-$(CH)_x$.

n_s is the number of impurities, R_{n,n_s} the distance between the nth carbon and the n_s impurities, d is the distance between the plane of the chain and the impurities, ε_1 and ε_2 are the dielectric constants parallel and perpendicular to the chain, and Λ is a constant. For the coulombic potential we used $\Lambda = 0.2$ Å^{-1}, $\varepsilon_1 = 7$, $\varepsilon_2 = 2$, $d = 2$ Å. The

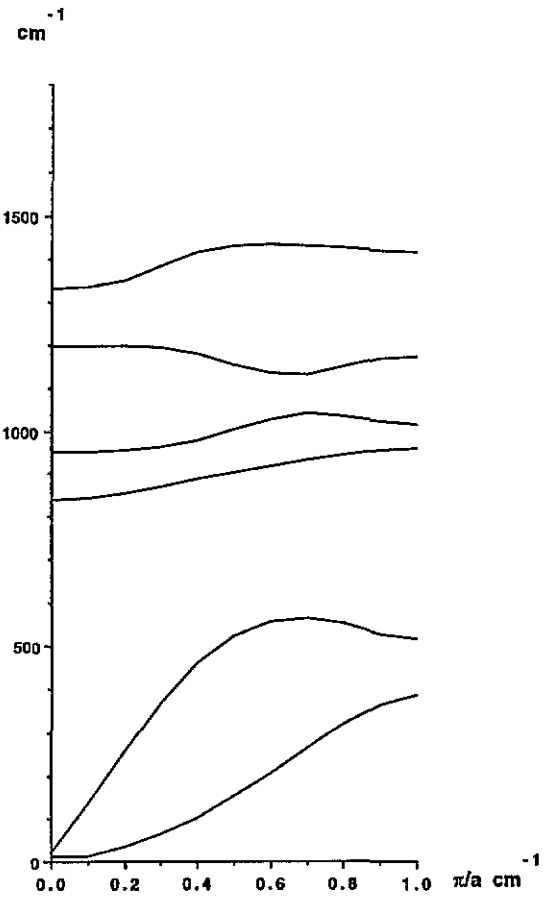

Figure 6. Dispersion curves for *trans*-$(CD)_x$.

conductivity of the doped $(CH)_x$ chain is reported in figure 7 for polarization parallel to the chain and in figure 8 for polarization perpendicular to the chain. For $(CD)_x$ results are reported in figure 9 for parallel polarization and figure 10 for perpendicular polarization.

For $(CH)_x$, figure 7 shows two intense peaks at 890 and 1395 cm^{-1}. For $(CD)_x$ we note two intense peaks at 760 and 1140 cm^{-1} and a shoulder at 1250 cm^{-1} (figure 9). These results agree very well with experiments. Note that one obtains with our model a natural width for the low-frequency peak. The width for this peak is generally interpreted as arising from a non-uniform distribution of the impurities (Horovitz 1982, Horovitz *et al* 1984, Zannoni and Zerbi 1982a, b). We note also that perpendicular conductivity is far from weak since the ratio between perpendicular and parallel conductivity is about 0.01. This result is in accordance with recent experimental results of Ali Benanamara (1992).

Without a pinning potential the peaks are found respectively at 500 cm^{-1} and 1380 cm^{-1}, so the shift from 500 cm^{-1} to 890 cm^{-1} is due to the coulombic pinning potential. This result explains why under strong doping the frequency of the 900 cm^{-1} mode does not shift below 500 cm^{-1} as it should do in the Horovitz model (Benoit *et al* 1983).

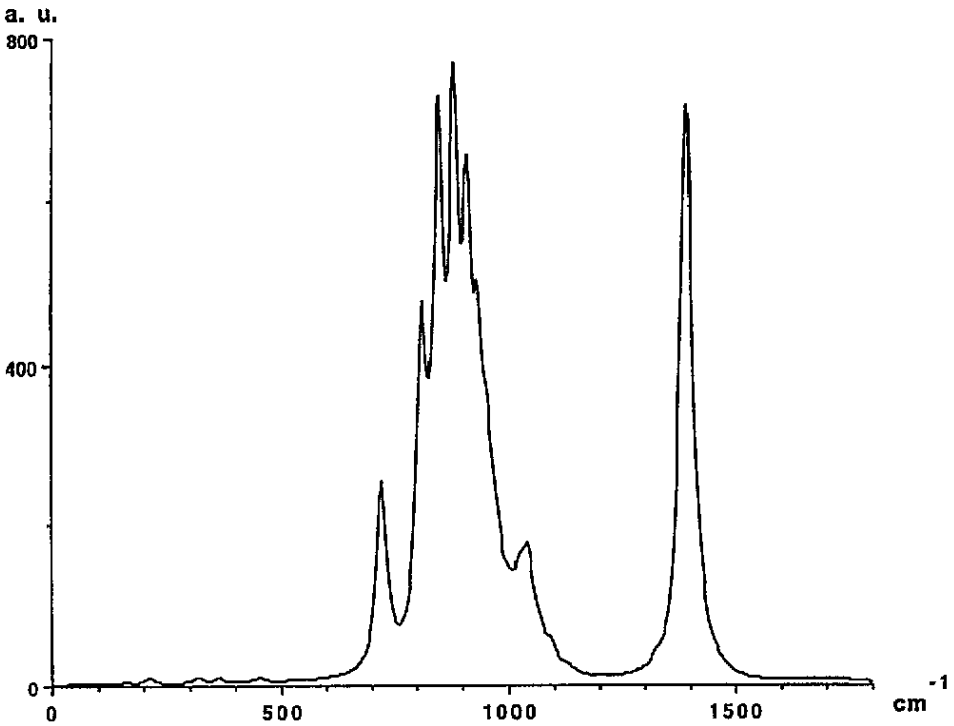

Figure 7. The IR conductivity of doped $(CH)_x$ for polarization parallel to the chain.

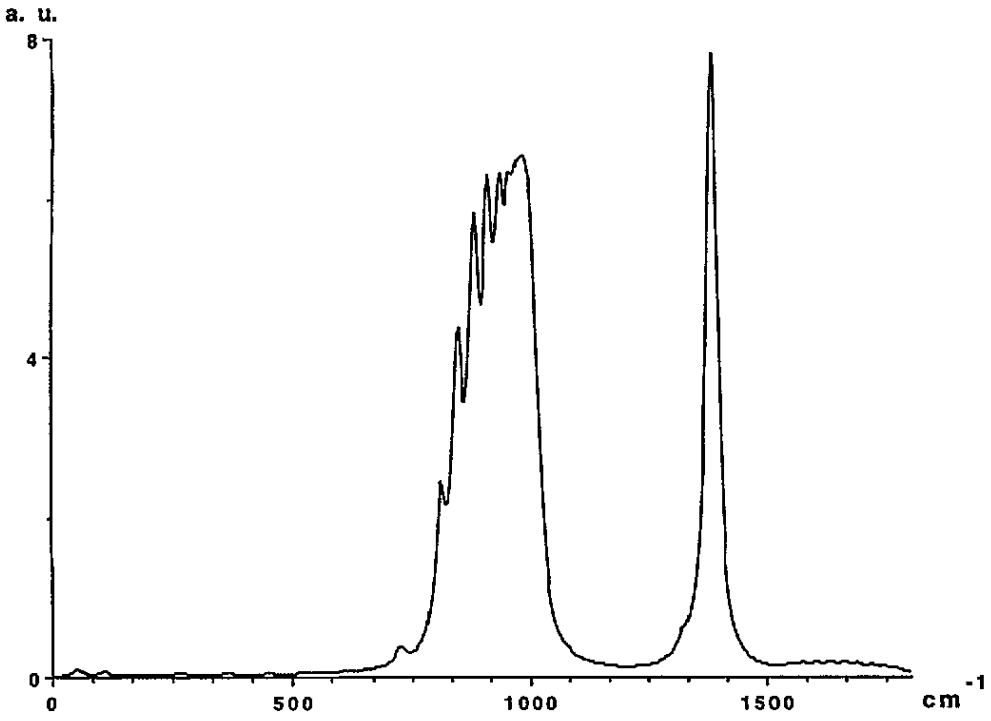

Figure 8. The IR conductivity of doped $(CH)_x$ for polarization perpendicular to the chain.

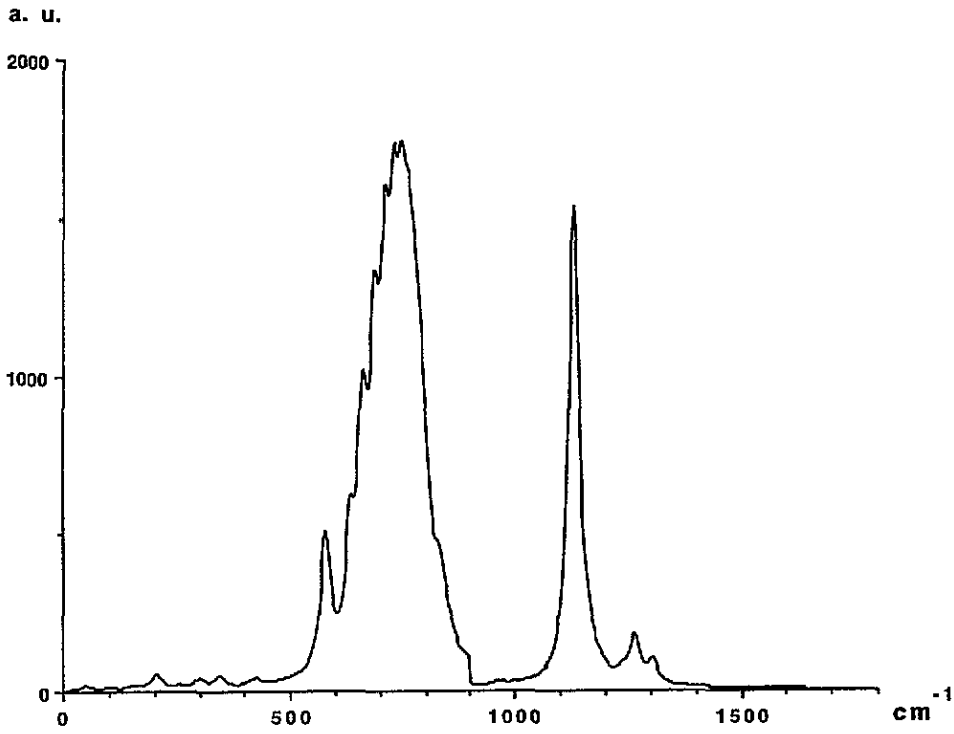

Figure 9. The IR conductivity of doped $(CD)_x$ for polarization parallel to the chain.

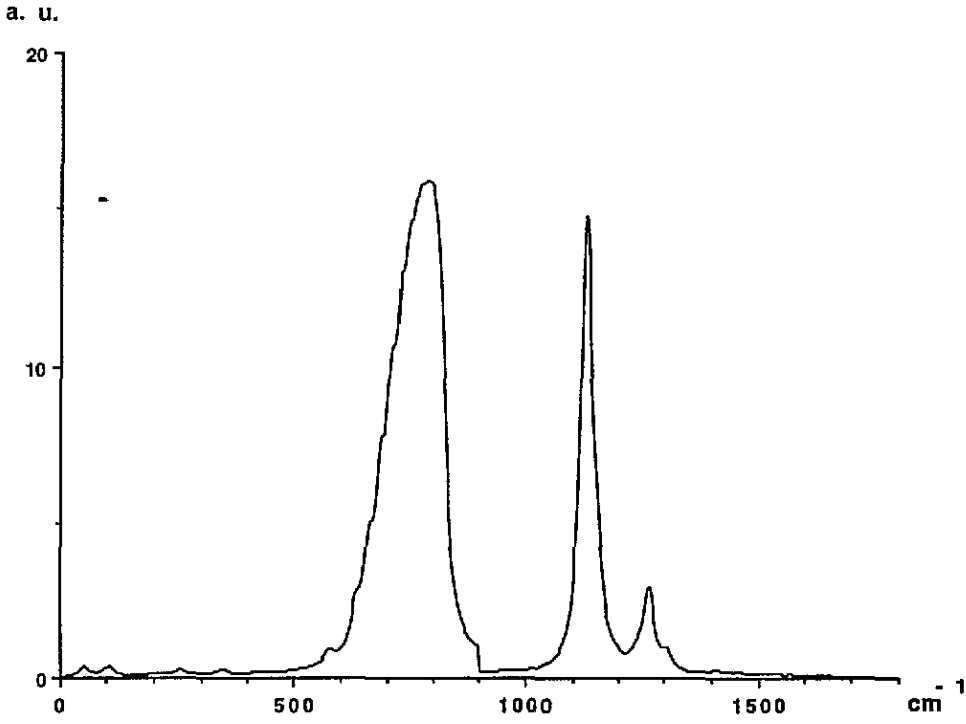

Figure 10. The IR conductivity of doped $(CD)_x$ for polarization perpendicular to the chain.

3. *Cis*-polyacetylene

For the *cis* isomer the Hamiltonian is given by

$$\mathbf{H}_{\text{cis}} = \mathbf{H}_{\text{cis}}^{\text{elect}} + \mathbf{H}_{\text{cis}}^{\text{elast}} + \frac{1}{2}\sum_{n,\alpha} m_n \dot{u}_{\alpha n}^2 \tag{38}$$

where the elastic Hamiltonian is given by

$$\mathbf{H}_{\text{cis}}^{\text{elast}} = \frac{1}{2}\sum_{ij} K'_{ij}\xi_i\xi_j \tag{39}$$

and the electronic Hamiltonian is given by (Springborg 1986a, b)

$$\begin{aligned}\mathbf{H}_{\text{cis}}^{\text{elect}} = &-\sum_{n,s} t_{n+1,n}(c_{n+1,s}^{+}c_{n,s} + c_{n,s}^{+}c_{n+1,s}) - \sum_{n,s} t'_{n,n+2}(c_{n,s}^{+}c_{n+2,s} + c_{n+2,s}^{+}c_{n,s}) \\ &- \sum_{n,s} t''_{2n+1,2n+4}(c_{2n+1,s}^{+}c_{2n+4,s} + c_{2n+4,s}^{+}c_{2n+1,s}) \\ &- \sum_{n,s} t'''_{2n,2n+3}(c_{2n,s}^{+}c_{2n+3,s} + c_{2n+3,s}^{+}c_{2n,s}).\end{aligned} \tag{40}$$

Parameters of the *cis* structure are taken such that $l_{C-C} = 1.46$ Å, $l_{C=C} = 1.34$ Å, $l_{C-H} = 1.09$ Å, $\theta(C=C-H) = 120°$, $\alpha(C=C-C) = 127.3°$. Table 4 gives values of the force constants deduced from the fit. Constants of the electronic Hamiltonian are $\alpha = 5.7$ eV Å^{-1}, $t_0 = 2.5$ eV, $u_0 = 0.032$ Å, $t' = 0.5$ eV, $t'' = 0.01$ eV, and $t''' = 0$ eV, which give a gap equal to 1.9 eV, in agreement with the experimental results. Experimental and theoretical results are reported in tables 5 and 6 for *cis*-$(CH)_x$ and *cis*-$(CD)_x$, respectively. We note that we obtain a good agreement. Our computation confirms that the B_{3u} mode, found at 1118 cm^{-1} by Galtier *et al* (1984) polarized along the chain, is a defect mode. The mode found at 1536 cm^{-1} certainly corresponds to the mode found by Piaggio *et al* (1984) at 1553 cm^{-1} which was not assigned. Dispersion curves of *cis*-$(CH)_x$ and *cis*-$(CD)_x$ are reported in figures 11 and 12, respectively.

Table 4. Elastic constants of *cis*-polyacetylene.

Force constants (mdyn Å^{-1}, mdyn, mdyn Å)			
$K(a_1^2)$	5.06	$K(\alpha_2^2)$	0.6
$K(a_2^2)$	7.7	$K(\alpha_1\alpha_2)$	−0.02
$K(a_1a_1)$	0.4	$K(\alpha_2\alpha_1)$	−0.18
$K(a_2a_2)$	0.6	$K(a_1\alpha_2)$	−0.12
$K(a_1a_2)$	0.68	$K(a_2\alpha_2)$	−0.25
$K(b_1^2)$	5.04	$K(\varphi_1^2)$	1.11
$K(a_1b_2)$	−0.06	$K(a_1\varphi_1)$	−0.27
$K(a_2b_2)$	−0.27	$K(a_2\varphi_1)$	−0.6

Table 5. Theoretical and experimental frequencies of *cis*-$(CH)_x$.

	Experimental frequencies		Theoretical frequencies	
	Galtier *et al* (1984)	Faulques (1990)	Faulques (1990)	Present work
	450	445	445	443
B_{1u}	1330	1330	1343	1346
	3045	3044	3025	3051
	Galtier *et al* (1984)	Faulques (1990)	Faulques (1990)	Present work
	1118 (def)	1115	1032	—
B_{3u}	1248	1247	1233	1247
	—	—	—	1536
	3058	3055	3055	3060
	Kuzmany (1980)	Faulques (1990)	Faulques (1990)	Present work
	1252	910	905	884
Ag	1292	1250	1249	1232
	1544	1540	1510	1555
	3090	3090	3107	3070
	Kuzmany (1980)	Faulques (1990)	Faulques (1990)	Present work
	445	446	434	435
B_{2g}	915	828	797	916
	1170	—	1250	1174
	3049	3030	3067	3053

Table 6. Theoretical and experimental frequencies of *cis*-$(CD)_x$.

	Experimental frequencies		Theoretical frequencies	
	Galtier *et al* (1984)	Faulques (1990)	Faulques (1990)	Present work
	402	402	405	408
B_{1u}	1049	1050	1047	1030
	2248	2255	2203	2244
	Galtier *et al* (1984)	Faulques (1990)	Faulques (1990)	Present work
	892	892	886	—
B_{3u}	798 (def)	947	1010	955
	—	—	—	1405
	2265	2275	2253	2267
	Kuzmany (1980)	Faulques (1990)	Faulques (1990)	Present work
	978	766	774	772
Ag	1205	975	977	994
	1460	1476	1497	1468
	2315	2315	2342	2306
	Kuzmany (1980)	Faulques (1990)	Faulques (1990)	Present work
	406	403	414	405
B_{2g}	870	—	769	850
	930	—	917	916
	2260	2260	2271	2264

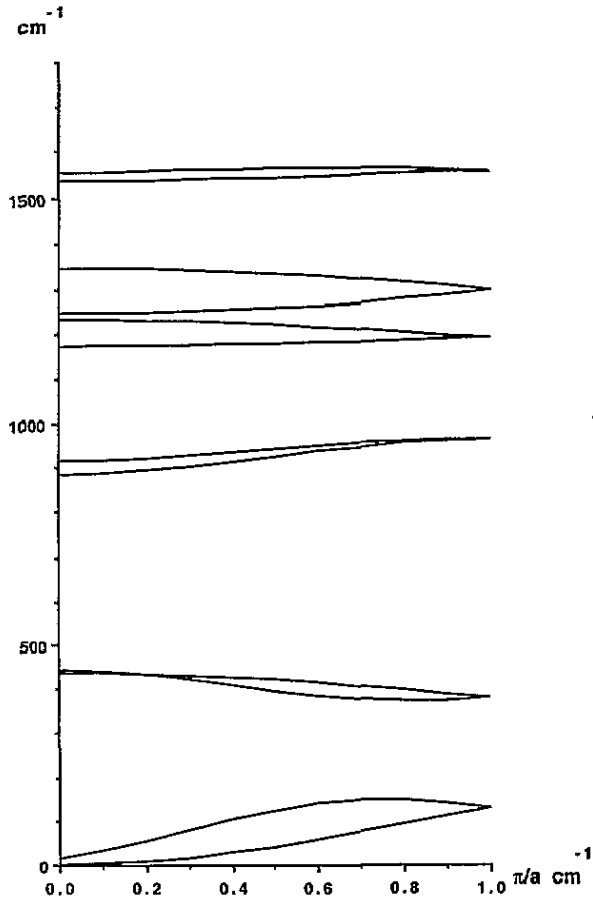

Figure 11. Dispersion curves for *cis*-$(CH)_x$.

4. *Cis–trans* defect

According to the work of Montaner *et al* (1981), Palpacuer *et al* (1982), and Gibson *et al* (1983, 1985), short sequences of *cis* persist in *trans*-polyacetylene even after long isomerization at high temperature. The Raman spectrum of the *trans* isomer is well interpreted in terms of short and long sequence length (Brivio and Mulazzi 1984). Such an interpretation is also in agreement with the persistence of *cis* sequences. In the photoinduced effect (Blanchet *et al* 1983, Vardeny *et al* 1983, 1986, Vardeny 1983, Schaffer *et al* 1987) peaks appear at 1370 cm^{-1}, 1260 cm^{-1}, and 500 cm^{-1} in $(CH)_x$ and 1045 cm^{-1}, 1225 cm^{-1}, and 400 cm^{-1} in $(CD)_x$. Weak peaks also appear at 1034 cm^{-1} and 1438 cm^{-1} in $(CH)_x$ and at 858 cm^{-1} and 1340 cm^{-1} in $(CD)_x$ (Vardeny *et al* 1986). Jones *et al* (1988) studied the decay of the IR absorption as a function of time after the exciting laser shut-off. They found decay half-lives of a few seconds and observed that half-lives decrease with increasing *trans* content.

The theory of photogeneration has been developed by several authors: Maki (1984) built a model where the interchain coupling is due to the hopping of the π electron. This coupling favours antiferromagnetic order between neighbouring chains and produces a confinement

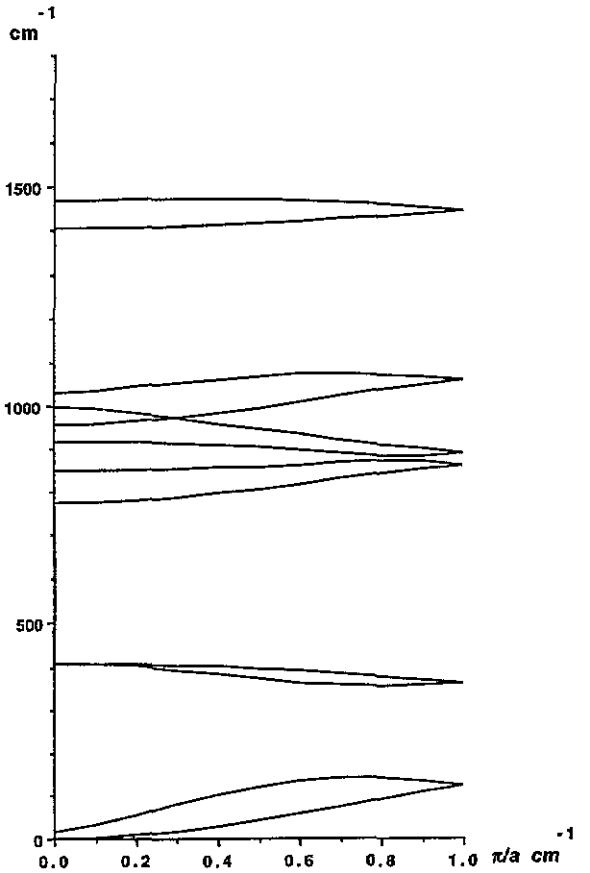

Figure 12. Dispersion curves for *cis*-$(CD)_x$.

of soliton pairs. To study the photogeneration, the author considers a pair of positively and negatively charged solitons S^+ and S^-. Calculating wave functions and energies for the lowest two states the author assigned the 500 cm^{-1} IR active mode found in photogeneration to the transition between the ground state and the first excited state of the S^+, S^- pair bound state. These results were discussed by Mele (1984) and Su (1987), who pointed out that the vibrational motion of this neutral exciton is not IR active and interpreted the photoinduced IR spectra as arising from an interchain pinning of solitons. Photogeneration has also been studied with the Horovitz (1982) formalism, where the pinning potential is now the coulombic attraction between charged solitons on adjacent chains. It was suggested by Su (1987) that a symmetry breaking on the chain could induce the photogeneration effect. We have proposed (Benoit *et al* 1990) that *cis–trans* defects could produce such a breaking. It was therefore very interesting to study the dynamical and optical properties of *cis–trans* defects in polyacetylene.

4.1. Neutral cis–trans defect

We consider a short *cis* sequence between two *trans* sequences (figure 13). For pure *cis* and *trans* regions we have used the force constants obtained with the perfect systems. For transition regions the force constants have been obtained by linear interpolation.

Computation has been performed with several lengths for pure *cis* and *trans* sequences. The results do not change for a *trans* sequence length higher than 80 carbon atoms. The best fits with experiment, classical IR absorption, and the photoinduced effect have been obtained for a pure *cis* sequence of 10 carbon atoms and a transition region of 23 carbon atoms. The classical IR absorption has been obtained with the usual expression for the imaginary part of the dielectric susceptibility

$$\chi''(\omega) = \frac{1}{2}\sum_j |C_{j\alpha}|^2 \frac{[\delta(\omega-\omega_j)-\delta(\omega+\omega_j)]}{2\omega_j} \tag{41}$$

where

$$C_{j\alpha} = \sum_n \frac{q_{\alpha n}}{\sqrt{m_n}} e_j(n,\alpha). \tag{42}$$

$q_{\alpha n}$ is the 'ionic' charge; $e_j(n,\alpha)$ is the (α,n)th component of the j mode. The IR conductivity induced by the defect, computed parallel and perpendicular to the chain, and the comparison with experiment are reported in figure 14. The numbers represent the experimental values of the frequency obtained by Piaggio *et al* (1984) but not interpreted. The agreement is very good and confirms the existence of this kind of defect. The results show that the peaks induced by the *cis–trans* defect at 465 cm^{-1}, 1248 cm^{-1}, 1378 cm^{-1}, and 1494 cm^{-1} correspond to the 443 cm^{-1}, 1247 cm^{-1}, 1346 cm^{-1}, and 1536 cm^{-1} modes of the *cis* isomer.

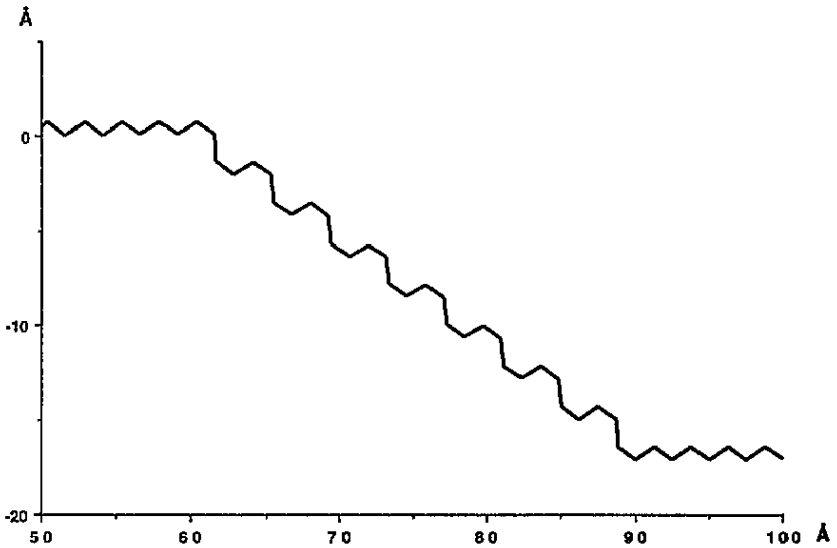

Figure 13. The structure of the *cis–trans* defect.

4.2. Cis–trans defect with neutral exciton

We propose to study the photoinduced IR activity in a system with a *cis–trans* defect, a positively charged soliton and a negatively charged antisoliton being placed on each side of the defect (neutral exciton).

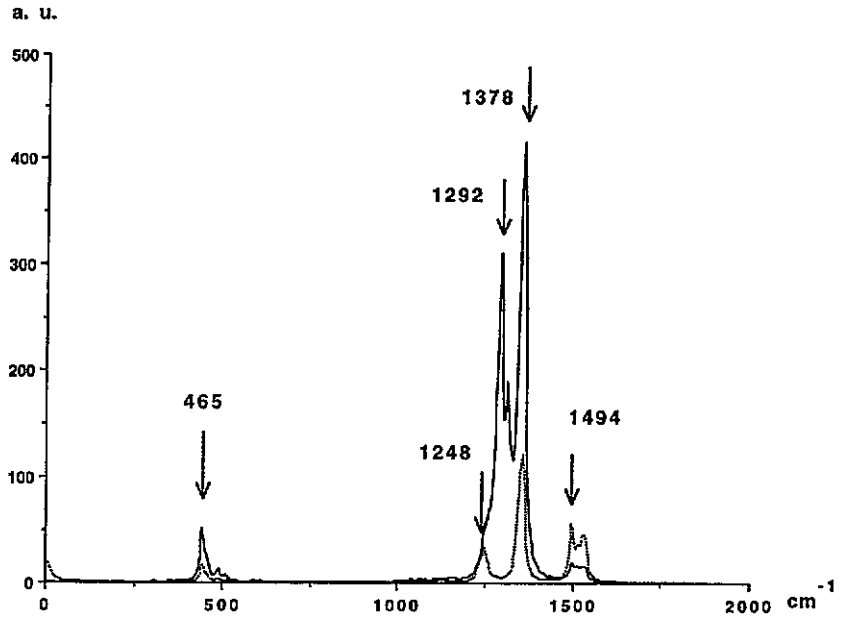

Figure 14. The IR conductivity induced by a neutral *cis–trans* defect: ——, parallel to the chain; - - - -, perpendicular to the chain. The IR conductivity for the pure *trans* and *cis* chains is not reported.

First we verified that in the absence of a *cis* sequence the IR activity was completely absent in accordance with the result of Mele (1984). To take into account the coulombic effect of the charged solitons we have used the following Hamiltonian:

$$\mathbf{H} = \mathbf{H}_{\text{trans}} + \mathbf{H}_{\text{cis}} + \mathbf{H}_{\text{cis-trans}} + V \tag{43}$$

where $\mathbf{H}_{\text{trans}}$, $\mathbf{H}_{\text{cis}}$, and $\mathbf{H}_{\text{cis-trans}}$ are respectively Hamiltonians of *trans*, *cis*, and *cis–trans* sequences. V represents the coulombic potential and is given by (Hicks and Tinka Gammel 1988)

$$V(n) = \frac{e^2}{\varepsilon_1\sqrt{\varepsilon_2}} \sum_{m^-} \frac{\rho(m^-) - \frac{1}{2}}{R_{n,m^-}} \exp(-\Lambda R_{n,m^-}) \tag{44}$$

where n is a soliton site and m^- an antisoliton site. R_{n,m^-} represents the distance between the site n and the site m.

We report in figures 15 and 16 the photoinduced activity parallel to the direction of the *trans* sequence for $(CH)_x$ and $(CD)_x$ respectively (Elmachtani-Idrissi 1993). We observe two intense peaks at 500 cm^{-1} and 1360 cm^{-1} and a weak peak at 1220 cm^{-1} for $(CH)_x$ and peaks at 410 cm^{-1}, 1080 cm^{-1}, and 1240 cm^{-1} for $(CD)_x$. We note that the width of the peak at 500 cm^{-1} is smaller than for the mode at 900 cm^{-1} in doped systems. We find also that perpendicular activity is very weak. The experimental peaks are reported in table 7 for comparison with our calculations. We can remark that our results are in good agreement with the experiments (Blanchet *et al* 1983, Vardeny *et al* 1983, Vardeny 1983, Schaffer *et al* 1987).

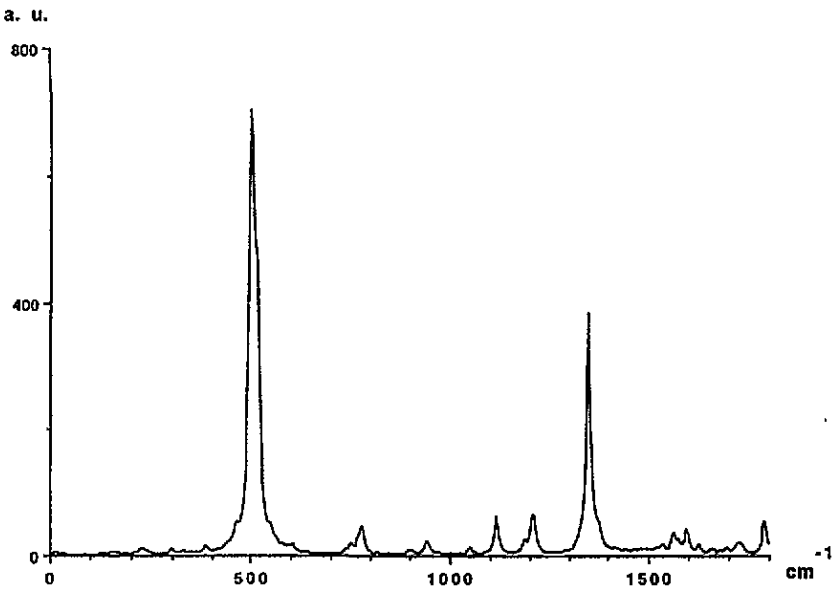

Figure 15. The photoinduced IR activity of the *cis–trans* $(CH)_x$ defect with a neutral exciton.

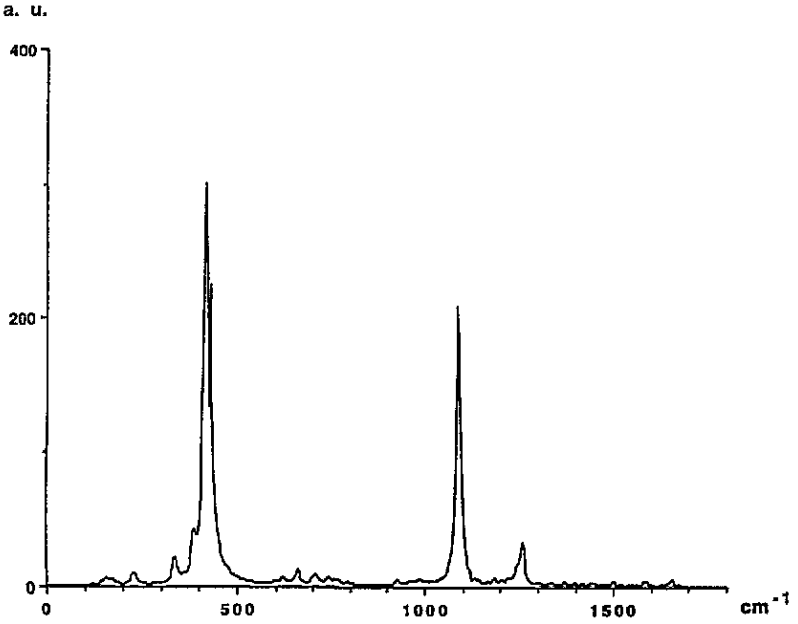

Figure 16. The photoinduced IR activity of the *cis–trans* $(CD)_x$ defect with a neutral exciton.

5. Conclusion

In this paper, we have developed realistic models for *cis* and *trans* structures of polyacetylene. Our models involve the real structure of the chain and the electron–phonon

Table 7. Theoretical and experimental frequencies for photoinduced activity of $(CH)_x$ and $(CD)_x$.

	Experimental frequencies			Theoretical frequencies
	Blanchet *et al* (1983)	Vardeny *et al* (1983)	Schaffer *et al* (1987)	Present work
$(CH)_x$	500	—	526	500
	1260	1260	1283	1220
	1370	1370	1365	1360
	Blanchet *et al* (1983)	Vardeny (1983)	Schaffer *et al* (1987)	Present work
$(CD)_x$	400	—	510	410
	1045	1045	1045	1080
	—	1225	1227	1240

coupling for both the isomers. The parameters of the models have been fitted with the perfect *cis* and *trans* systems. These values have been used to study the IR activity of the doped chain. We found that the coulombic potential not only shifts the Goldstone mode towards high frequency but also induces an increase of the width of this mode. We found also that the perpendicular conductivity is not weak. This effect arises from the zig-zag structure of the chain. We have also studied a *cis–trans* defect. We assumed that this defect is planar, which is certainly not true in real systems. However the study of the neutral defect has allowed us to explain the origin of some IR peaks without any adjustment of the parameters of the model. The study of the conductivity of the neutral chain with a pair of soliton and an antisoliton has shown that this system becomes IR active when the soliton and the antisoliton are significant charges with opposite sign. In fact the charges are placed in the valence band and in the first level in the gap. If we evaluate the charge of the soliton (or antisoliton) we find that this charge is about $0.9e$ depending on the relative position of the soliton–antisoliton pair with respect to the defect. This could explain the dependence of the decay time on the length of the *cis* sequence (*cis–trans* ratio).

References

Abrikosov A A, Gorkov L P and Dzyaloshinski I E 1963 *Method of Quantum Field Theory in Statistical Physics* ed R A Silverman (Englewood Cliffs, NJ: Prentice-Hall)

Ali Benanamara A 1992 *Thèse* Université de Montpellier

Baughman R H and Moss G 1982 *J. Chem. Phys.* **77** 6321

Benoit C, Bernard O, Palpacuer M, Rolland M and Abadie M J M 1983 *J. Physique* **44** 1307

Benoit C, Rolland M and Palpacuer M 1990 *Phys. Status Solidi* **162** 9

Benoit C, Royer E and Poussigue G 1992 *J. Phys.: Condens. Matter* **4** 3125

Blanchet G B, Fincher C R, Chung T C and Heeger A J 1983 *Phys. Rev. Lett.* **50** 1938

Brivio G P and Mulazzi E 1984 *Phys. Rev.* B **30** 876

Chao K A and Wang Y 1985 *J. Phys. C: Solid State Phys.* **18** L1127

Elmachtani-Idrissi J 1993 *Thèse* Université de Montpellier

Faulques E 1990 *Thèse d'état* Université de Nantes

Galtier M, Charbonnel M, Montaner A and Ribet J L 1984 *Polymer* **25** 253

Gibson H W, Weagley R J, Mosher R, Kaplan S, Prest W M Jr and Epstein A J 1985 *Phys. Rev.* **31** 2338

Gibson H W, Weagley R J, Prest W M Jr, Mosher R and Kaplan S 1983 *J. Physique Coll.* **44** C3 123

Heeger A J, Kivelson S, Schrieffer J R and Su W P 1988 *Rev. Mod. Phys.* **60** 781

Hicks J C and Blaisdell G A 1985 *Phys. Rev.* B **31** 919

Hicks J C and Mele E J 1986 *Phys. Rev.* B **34** 1091

Hicks J C and Tinka Gammel J 1986 *Phys. Rev. Lett.* **57** 1320

—— 1988 *Phys. Rev.* B **37** 6315

Hicks J C, Tinka Gammel J, Han-Yong Choi and Mele E J 1987 *Synth. Met.* **17** 57
Horovitz B 1982 *Solid State Commun.* **41** 729
Horovitz B, Vardeny Z, Ehrenfreund E and Brafman O 1984 *Synth. Met.* **9** 215
Ito H and Ono Y 1985 *J. Phys. Soc. Japan* **54** 1194
Ito H, Terai A, Ono Y and Wada Y 1984 *J. Phys. Soc. Japan* **53** 3520
Jones T E, Schindler J W, Mosier-Boss P A, Bendall C S, Smith C A, Boss R D, Hicks J C and Lambert L M 1988 *Phys. Rev.* B **37** 10814
Kim Y H and Heeger A J 1989 *Phys. Rev.* B **40** 8393
Kuwabara M and Ono Y 1993 *J. Phys. Soc. Japan* **62** 990
Kuzmany H 1980 *Phys. Status Solidi* b **97** 521
Maki K 1984 *Synth. Met.* **9** 185
Matsubara T 1956 *Prog. Theor. Phys.* **14** 351
Mele E J 1981 *Mol. Cryst. Liq. Cryst.* **77** 25
—— 1984 *Solid State Commun.* **49** 555
Mele E J and Hicks J C 1985 *Phys. Rev.* B **32** 2703
Mele E J and Rice M J 1980 *Phys. Rev. Lett.* **45** 926
Montaner A, Galtier M, Benoit C and Aldissi M 1981 *Solid State Commun.* **39** 99
Mulazzi E, Brivio G P, Faulques E and Lefrant S 1983 *Solid State Commun.* **46** 851
Nakahara M and Maki K *1982 Phys. Rev.* B **25** 7789
Palpacuer M, Bernard O, Deloupy C, Rolland M and Abadie M J M 1982 *Polymer* **23** 1847
Piaggio P, Dellepiane G, Piseri L, Tubino R and Tiliani C 1984 *Solid State Commun.* **50** 947
Schaffer H E, Friend R H and Heeger A J 1987 *Phys. Rev.* B **36** 7537
Schügerl F B and Kuzmany H 1981 *J. Chem. Phys.* **74** 953
Shirakawa H and Ikeda S 1971 *Polymer* **2** 231
Shuai Z, Brédas J L and Sun X 1993 *Phys. Rev.* B **47** 13260
Sprinborg M 1986a *Phys. Rev.* B **33** 8475
—— 1986b *Phys. Scr.* **13** 306
Su W P 1987 *Phys. Rev.* B **35** 9245
Su W P, Schrieffer J R and Heeger A J 1979 *Phys. Rev. Lett.* **42** 1698
—— 1980 *Phys. Rev.* B **23** 2099
Sun X, Wu C and Shen X C 1985 *Solid State Commun.* **56** 1039
Takayama M, Lin-Liu Y R and Maki K 1980 *Phys. Rev.* B **21** 2388
Terai A, Ito H, Ono Y and Wada Y 1985a *J. Phys. Soc. Japan* **54** 196
—— 1985b *J. Phys. Soc. Japan* **54** 4468
Terai A and Ono Y 1986 *J. Phys. Soc. Japan* **55** 213
Terai A, Ono Y and Wada Y 1986 *J. Phys. Soc. Japan* **55** 2889
Vardeny Z 1983 *Phys. Rev. Lett.* **51** 1221
Vardeny Z, Ehrenfreund E, Brafman O, Horovitz B, Fujimoto H, Tanaka J and Tanaka M 1986 *Phys. Rev. Lett.* **57** 2995
Vardeny Z, Orenstein J and Baker G L 1983 *Phys. Rev. Lett.* **50** 2032
Zannoni G and Zerbi G 1982a *Chem. Phys. Lett.* **87** 50
—— 1982b *Chem. Phys. Lett.* **87** 55
Zhen Ye 1992 *Phys. Status Solidi* b **174** 393